

Scaling behavior in convection-driven Brazil-nut effect

Prakhyat Hejmady,^{*} Ranjini Bandyopadhyay,[†] Sanjib Sabhapandit,[‡] and Abhishek Dhar[§]
Raman Research Institute, CV Raman Avenue, Sadashivanagar, Bangalore 560080, India

(Dated: October 30, 2018)

The Brazil-nut effect is the phenomenon in which a large intruder particle immersed in a vertically shaken bed of smaller particles rises to the top, even when it is much denser. The usual practice, while describing these experiments, has been to use the dimensionless acceleration $\Gamma = a\omega^2/g$, where a and ω are respectively the amplitude and the angular frequency of vibration and g is the acceleration due to gravity. Considering a vibrated quasi-two-dimensional bed of mustard seeds, we show here that the peak-to-peak velocity of shaking $v = a\omega$, rather than Γ , is the relevant parameter in the regime where boundary-driven granular convection is the main driving mechanism. We find that the rise-time τ of an intruder is described by the scaling law $\tau \sim (v - v_c)^{-\alpha}$, where v_c is identified as the critical vibration velocity for the onset of convective motion of the mustard seeds. This scaling form holds over a wide range of (a, ω) , diameter and density of the intruder.

Besides its obvious technological importance, granular matter is one of the most interesting examples of a driven dissipative system. Shaken granular matter exhibits various phenomena such as convection, segregation and jamming. A striking experimental observation in vibrated granular materials is the Brazil-nut effect (BNE), where a large intruder particle immersed in a vertically shaken bed of smaller particles rises to the top, even when it is much denser [1–8]. A related effect is the segregation obtained on vibrating a mixture of particles of different sizes and densities. While some progress has been made, a complete understanding of these observations is still lacking. The consensus now is that different segregation mechanisms such as convection, void filling, air-drag and kinetic-energy driven methods are responsible for the effect, each being dominant in different parameter regimes [2–4, 9, 10]. In this Letter, we show that in a broad parameter regime where convection is responsible for BNE, the driving velocity $v = a\omega$ is the relevant scaling variable rather than the commonly used dimensionless acceleration $\Gamma = a\omega^2/g$. Here, a and ω are respectively the amplitude and angular frequency of vibration and g is the acceleration due to gravity. This is demonstrated through a very good collapse of the rise-time data as a function of the driving velocity.

It is well known that granular convection can be either boundary wall-driven [7] or buoyancy-driven [16]. Boundary-driven convection is unique to granular systems and refers to the case where the surface properties of the side walls and their shape are crucial in determining the formation and nature of the convection rolls [11–14]. Buoyancy-driven granular convection, on the other hand, is seen under strong driving and is analogous to Rayleigh-Benard convection in fluids [15–17].

In this Letter, our focus is on boundary-driven convection. One of the simplest measurements in a granular convecting fluid is that of the rise-time τ of a large intruder. This quantity effectively provides a single observable characterizing the complex velocity field in the system. The intruder rise-time has been used as a probe for understanding the effects of driving frequency and amplitude, interstitial air-flow, the size and density of the intruder, and wall effects on BNE. Duran *et al.* [5] studied BNE in a quasi-two-dimensional bed of aluminium

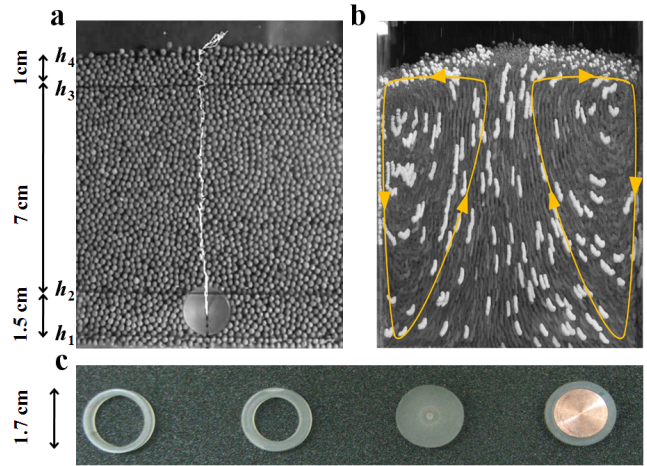


FIG. 1: (Color online) Experimental setup. **a**. The initial position of an acrylic intruder of diameter 1.7 cm embedded in a column of mustard seeds of sizes between 1.5 mm and 2 mm. The bottom of the intruder is placed at a height $h_1 = 5$ mm from the floor of the cell. The rise-time τ is the time taken by the centre of the intruder to move from the height h_2 to the height h_3 . A typical trajectory of the rising intruder is shown by the vertical white line. **b**. Convection pattern obtained by superposing many consecutive time-lapsed images of the vibrated bed of black mustard seeds in which yellow mustard seeds are distributed randomly to serve as tracer particles. The two loops (yellow) with arrows indicate the flow direction of the mustard seeds. **c**. Intruders used in the experiment with relative densities ranging between 0.30 – 2.34.

beads. They demonstrated two different segregation mechanisms: arching effects were found to dominate in the range $\Gamma_c < \Gamma \lesssim 1.5$ with $\Gamma_c \approx 1$, while convection gives rise to segregation at $\Gamma \gtrsim 1.5$. In the arching regime, intruder rise was observed only when intruder-to-bead diameter ratio was large enough. In the convective regime, the rise-time was independent of intruder diameter. For a three-dimensional bed of glass beads, the rise-time of tracer particles in the boundary-driven convection regime was studied in [7]. For a *fixed* driving frequency, a $\tau \sim (\Gamma - \Gamma_c)^{-2.5}$ dependence with $\Gamma_c \approx 1.2$ was reported, while for fixed Γ values, an exponential dependence



FIG. 2: (Color online) A series of snapshots of the vibrated bed taken at regular intervals of 8 seconds. Top and bottom panels are for experiments done without and with an intruder respectively. The shaking parameters were set at $f = 50$ Hz and $a = 1.6$ mm. In the bottom panel, the intruder diameter is 1.7 cm and $\rho_r = 1.07$. The alternate black and yellow mustard layers initially destabilize at the walls and eventually bulk convection rolls are formed. An inspection of these figures confirms that the granular convection patterns do not change significantly as a result of the presence of the intruder, except close to the intruder boundary.

on frequency was obtained. In a later work, Vanel *et al.* [8] looked at the motion of an intruder and reported deviations from the above behaviour. However, none of these studies have obtained any scaling of the rise-time data. An understanding of the dependence of rise-time on driving amplitude and frequency therefore remains incomplete.

The present work reports experimental measurements of the rise-time of an intruder in a vertically vibrated quasi-two-dimensional bed of mustard seeds (Fig. 1). The experimental setup consists of a quasi-two-dimensional rectangular acrylic cell of height 25 cm, width 13 cm and gap 6 mm. The cell is filled up to a height h with black mustard seeds of density 1.11 g/cc and sizes between 1.5 and 2 mm. The intruder is a large acrylic disk of diameter 1.7 cm, thickness 5 mm and density 1.07 g/cc. The thickness of the intruder is chosen such that mustard seeds are not able to enter the space between the intruder and the cell walls. The cell is mounted on a 50 kgf DESPL electrodynamic shaker executing vertical sinusoidal vibrations of the required amplitudes and frequencies. The narrow side walls of the cell are roughened by lining them with fine sandpaper (ISO grit designation $P - 100$). For these boundary conditions, the experiments were reproducible. However, for smooth walls it was found that the convection patterns were irreproducible and often the system would jam. The humidity of the lab was maintained at 40%.

In order to produce fixed initial conditions corresponding roughly to a fixed spatial distribution of mustard seeds, the cell was initially vibrated at a high Γ and the intruder was pushed to a fixed depth h_1 (Fig. 1a). The driving was then removed and the top layer leveled. The cell was then vibrated at the required amplitude and frequency ($f = \omega/2\pi$). The upward motion of the intruder was recorded using a Panasonic Lumix DMC-TZ3 digital camera at a rate of 33 frames/sec. The tracking of the intruder (Fig. 1a) was done using a Labview based particle tracking algorithm [18]. In order to change the density of the intruder, several acrylic in-

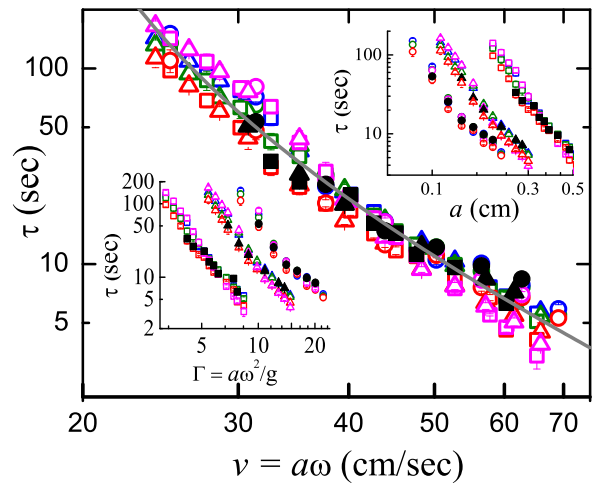


FIG. 3: (Color online) Intruder rise-time plots. Upper inset: Plots of the rise-time τ versus shaking amplitude a for different frequencies: i) 20 Hz (\square) ii) 35 Hz (\triangle) and iii) 50 Hz (\circ) for an intruder of diameter 1.7 cm and for four different relative densities $\rho_r = 0.3$ (blue), 0.8 (green), 1.07 (red) and 2.34 (magenta). The filled symbols correspond to a 1 cm diameter intruder with $\rho_r = 1.07$. Lower inset: Plot of the same data versus the dimensionless acceleration Γ . Main figure: Plot of τ versus peak-to-peak velocity of shaking $v = a\omega$. The data collapses for the entire range of shaking velocities, for all relative densities and for the two intruder sizes. The solid line shows the functional form $\tau \sim (v - v_c)^{-\alpha}$ with $\alpha = 2.0$ and $v_c = 16$ cm/sec.

truders with holes in the centre were made. By changing the size of the holes or inlaying them with copper, a range of density ratios $\rho_r = (\text{intruder density})/(\text{mustard seed density})$ between 0.30 and 2.34 (Fig. 1c) was achieved: $\rho_r = 0.3$ for acrylic with 1.4 cm air hole, 0.8 for acrylic with 1.2 cm air hole, 1.07 for solid acrylic disk and 2.34 for acrylic with 0.65 cm copper. The rise-time of the intruder was computed by estimating the time taken by it to rise from a fixed starting position h_2 to a fixed final position h_3 (Fig. 1a). The mean rise-time τ was computed by averaging over 10 trials for every parameter set.

The measurements were made under a fairly wide range of driving parameters, obtained by varying frequencies and amplitudes ($2.5 \lesssim \Gamma \lesssim 25$), intruder densities and diameters. Shaking the bed vertically results in a thin downward moving layer of mustard seeds adjacent to each side wall, which sets up bulk upward motion elsewhere in the system as seen in Fig. 1(b). This convective motion of the medium carries the intruder to the top of the bed. The granular convection phenomenon was studied in greater detail by filling up the rectangular cell with alternating layers of black and yellow mustard seeds, with each layer being approximately 2 cm thick. In Fig. 2 we see that for a given set of shaking parameters, very similar flow patterns of the medium are obtained with and without the intruder

Next, we measure the rise-times τ for several peak-to-peak

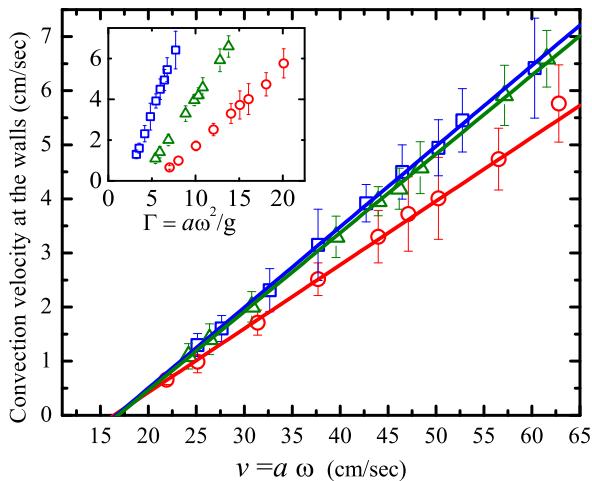


FIG. 4: (Color online) Convection velocities at the side walls. The convection velocities, in the absence of the intruder, are plotted versus the peak-to-peak velocity of shaking $v = a\omega$ for shaking frequencies: i) 20 Hz (\square), ii) 35 Hz (\triangle) and iii) 50 Hz (\circ). Each linear fit (denoted by solid line) is extrapolated to estimate the peak-to-peak shaking velocity for the onset of convection. The x -intercepts lie in the range of 16 – 17 cm/sec. Inset: Plot of the convection velocities at the side-wall as a function of Γ .

amplitudes and frequencies and for various relative densities ρ_r . The rise-time decreases with increasing shaking frequencies and amplitudes, as seen in the upper inset of Fig. 3. It is observed that τ is almost independent of density over the range used in these experiments ($\rho_r = 0.30 - 2.34$). This is in contrast to the three-dimensional results [3, 19, 20] where a non-monotonic dependence of τ on ρ_r was found. There is no scaling of τ with Γ (lower inset of Fig. 3). In contrast, a plot of τ as a function of the shaking velocity $v = a\omega$ (Fig. 3) shows an excellent collapse of the data. Throughout the parameter regime where the collapse holds, we find that boundary driven convection is the dominant mechanism responsible for the rise of the intruder. This collapse holds for the entire range of intruder densities and the two intruder sizes (diameters 1.7 cm and 1 cm) that were used. The intruder therefore behaves approximately like a massless tracer particle tracking the convective flow of the background granular medium. The collapsed τ -vs- v data of Fig. 3 is well described by the scaling-law $\tau = A(v - v_c)^{-\alpha}$, where $\alpha = 2.0$ and A , v_c are fitting parameters. For the range of ρ_r values investigated, v_c is found to be around 15 – 18 cm/sec and A is around $13,000 \pm 500 \text{ cm}^2/\text{sec}$. We note that v has been used as a scaling parameter in the vibro-fluidized regime [15–17] that is typically realized at much higher driving ($\Gamma \gtrsim 50$) and is *not* wall-driven. It has also been noted in experiments on granular compaction by tapping that v , rather than Γ , is the appropriate control parameter [21]. However, no scaling has been achieved so far in the boundary-driven convection regime. Given the non-homogeneous flow fields that are set up in our experiments, the dependence of τ on shaking veloc-

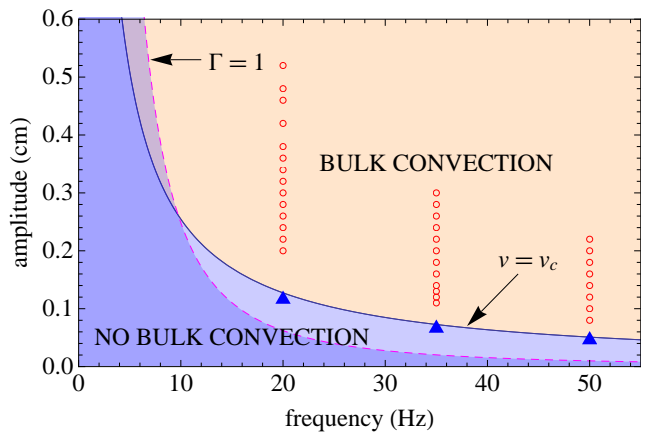


FIG. 5: (Color online) Phase diagram. Each data point (\circ) corresponds to a set of (amplitude, frequency) parameter values for which BNE was observed in our experiments, while the points (\blacktriangle) represent data sets where no bulk convection, and therefore no BNE, was observed. The solid line corresponds to $v = a(2\pi f) = v_c$, while the dashed line corresponds to $\Gamma = a(2\pi f)^2/g = 1$. Bulk convection occurs only in the region where both the conditions $\Gamma > 1$ and $v > v_c$ are satisfied.

ity is rather surprising.

The absence of any dependence of the rise-time of the intruder on its size and density implies that convection is the dominant driving mechanism. To confirm this premise, we make an independent measurement of the convection velocity of the mustard seeds without the intruder. For measuring the convection velocity at the wall, tagged particles (yellow mustard seeds of sizes and densities lying within the same range as the black mustard seeds) were distributed randomly in the bed of black mustard seeds. Over a range of shaking frequencies and amplitudes, we measured the velocity of these tagged particles moving down the two side walls (supplementary material). High speed tracking of mustard-seed convection at the side walls was done using an IDT MotionPro high speed camera at a rate of 150 frames/sec. The velocity of the boundary layer particles is an order of magnitude larger than the mean velocity of the intruder. As shown in Fig. 4, the convection velocities measured by this procedure show a much better data-collapse when plotted against $v = a\omega$ than when plotted as a function of Γ . A linear extrapolation of the data to zero convection velocity gives a critical velocity of 16 – 17 cm/sec for the onset of convection. This critical velocity range overlaps with the range of the fitting parameter v_c obtained from the rise-time data. It is therefore natural to identify v_c as the critical shaking velocity required for the onset of convection cycles in the granular column.

Our understanding of the different parameter regimes for boundary driven convection is summarized in the phase diagram in Fig. 5. We note that while $\Gamma > 1$ is necessary for bulk convection, it is not a sufficient condition. As seen in the phase diagram, there is a region of parameter values, with $\Gamma > 1$ and $v < v_c$, where no bulk convection occurs. In exper-

iments performed in this regime, we observed some motion of the mustard seeds restricted entirely to the the upper corners of the bed. Such a condition cannot give rise to BNE for the intruder sizes studied here. We expect that for much larger intruder sizes, other mechanisms may come into play which can drive BNE [5]. We have verified (supplementary material) that the scaling of rise-time continues to hold for different bed-widths, wall roughness and for choice of bed-particles. We also find that on varying the bed-height, the scaling holds for smaller heights (supplementary material) but breaks down for larger heights. The microscopic origins of the parameters α , A and v_c are not clear as they depend on the cell geometry which is easily characterizable, as well as on details such as the wall, and bed-particle roughness, which are harder to characterize.

The scaling dependence of the velocity and the rise-time on the shaking velocity $a\omega$ can roughly be understood by analyzing the hydrodynamical equations that have been earlier used to describe vibrated granular systems. In our case, the system is nearly incompressible in the bulk and hence the appropriate equations for the velocity field $\mathbf{u}(x, y)$ and the granular temperature $T(x, y)$, in the steady state, are [17, 22, 23]

$$\mathbf{u} \cdot \nabla \mathbf{u} = -\frac{1}{\rho} \nabla p + \nu \nabla^2 \mathbf{u} + g \hat{\mathbf{g}} \quad (1)$$

$$\mathbf{u} \cdot \nabla T = \nabla \cdot (\kappa \nabla T) - I, \quad (2)$$

where ρ is the ‘‘granular fluid’’ density, the pressure $p/\rho \propto T/m$ and the viscosity and thermal conductivity are given by $\nu \propto \kappa = (0.6\ell + d)^2 \ell^{-1} \sqrt{T/m}$, with ℓ and d being the mean free path and particle diameter respectively. The energy dissipation is given by the term $I \propto \ell^{-1} T \sqrt{T/m}$. With a rescaling of the variables $\mathbf{u} \rightarrow (a\omega)\mathbf{u}$, $\{p/\rho, T/m\} \rightarrow (a\omega)^2 \{p/\rho, T/m\}$ and $\nabla \rightarrow b^{-1} \nabla$, where b is some typical coarsening length scale, the above equations transform to

$$\mathbf{u} \cdot \nabla \mathbf{u} = -\frac{1}{\rho} \nabla p + \frac{\nu}{b} \nabla^2 \mathbf{u} + \frac{b}{a} \frac{\hat{\mathbf{g}}}{\Gamma} \quad (3)$$

$$\mathbf{u} \cdot \nabla T = \frac{1}{b} \nabla \cdot (\kappa \nabla T) - bI. \quad (4)$$

For large Γ , the last term in Eq. (3) can be neglected, and the scaled equations become independent of a and ω . This may explain the scaling behaviour of velocities with $a\omega$ seen in our experiments.

Finally, we anticipate that a similar scaling should hold even in three-dimensional granular systems in some parameter regime where granular convection is the dominant mechanism driving the BNE. We note that since the experiments in [7] were performed at a fixed frequency, their result $\tau \sim (\Gamma - \Gamma_c)^{-2.5}$ is consistent with our scaling form $\tau \sim (v - v_c)^{-\alpha}$ with $\alpha = 2.5$.

The authors thank P. Nandakishore and D. Saha for their help with the experiments. We thank N. Menon and D. J. Durian for useful discussions.

* Electronic address: phejmady@rri.res.in

† Electronic address: ranjini@rri.res.in

‡ Electronic address: sanjib@rri.res.in

§ Electronic address: dabhi@rri.res.in

- [1] A. Rosato, K. J. Strandburg, F. Prinz, and R. H. Swendsen, Phys. Rev. Lett. **58**, 1038 (1987).
- [2] H.M. Jaeger, S.R. Nagel, and R.P. Behringer, Rev. Mod. Phys. **68**, 1259 (1996).
- [3] M. E. Möbius, B.E. Lauderdale, S.R. Nagel, and H.M. Jaeger, Nature (London) **414**, 270 (2001).
- [4] A. Kudrolli, Rep. Prog. Phys. **67**, 209 (2004).
- [5] J. Duran, T. Mazozi, E. Clément, and J. Rajchenbach, Phys. Rev. E **50**, 5138 (1994).
- [6] K. Liffman *et al.*, Granular Matter **3**, 205 (2001).
- [7] J. B. Knight, E. E. Ehrichs, V. Y. Kuperman, J. K. Flint, H. M. Jaeger and S. R. Nagel, Phys. Rev. E **54**, 5726 (1996).
- [8] L. Vanel, A. D. Rosato, and R. N. Dave, Phys. Rev. Lett. **78**, 1255 (1997).
- [9] W. Cooke, S. Warr, J. M. Huntley, and R. C. Ball, Phys. Rev. E **53**, 2812 (1996).
- [10] M. Schröter, S. Ulrich, J. Kreft, J. B. Swift, and H. L. Swinney, Phys. Rev. E **74**, 011307 (2006).
- [11] J. B. Knight, H. M. Jaeger and S. R. Nagel, Phys. Rev. Lett. **70**, 3728 (1993).
- [12] J. B. Knight, Phys. Rev. E **55**, 6016 (1997).
- [13] M. Bourzutschky and J. Miller, Phys. Rev. Lett. **74**, 2216 (1995).
- [14] E. E. Ehrichs, H. M. Jaeger, G. S. Karczmar, J. B. Knight, V. Y. Kuperman and S. R. Nagel, Science **267**, 1632 (1995).
- [15] P. Eshuis, K. van der Weele, D. van der Meer, and D. Lohse, Phys. Rev. Lett. **95**, 258001 (2005).
- [16] P. Eshuis, K. van der Weele, D. van der Meer, R. Bos and D. Lohse, Phys. Fluids **19**, 123301 (2007).
- [17] P. Eshuis, D. van der Meer, M. Alam, K. van der Weele and D. Lohse, Phys. Rev. Lett. **104**, 038001 (2010).
- [18] <http://grahammilne.com/tracker.htm>
- [19] M. E. Möbius, X. Cheng, G. S. Karczmar, S. R. Nagel, and H. M. Jaeger, Phys. Rev. Lett. **93**, 198001 (2004).
- [20] M. E. Möbius, X. Cheng, P. Eshuis, G. S. Karczmar, S. R. Nagel, and H. M. Jaeger, Phys. Rev. E **72**, 011304 (2005).
- [21] J. A. Dijksman and M. van Hecke, Euro. Phys. Lett. **88**, 44001 (2009).
- [22] E. L. Grossman, T. Zhou, and E. Ben-Naim, Phys. Rev. E **55**, 4200 (1997).
- [23] B. Meerson, T. Pöschel, and Y. Bromberg, Phys. Rev. Lett. **91**, 024301 (2003).

Supplementary material for “Scaling behavior in convection-driven Brazil-nut effect”

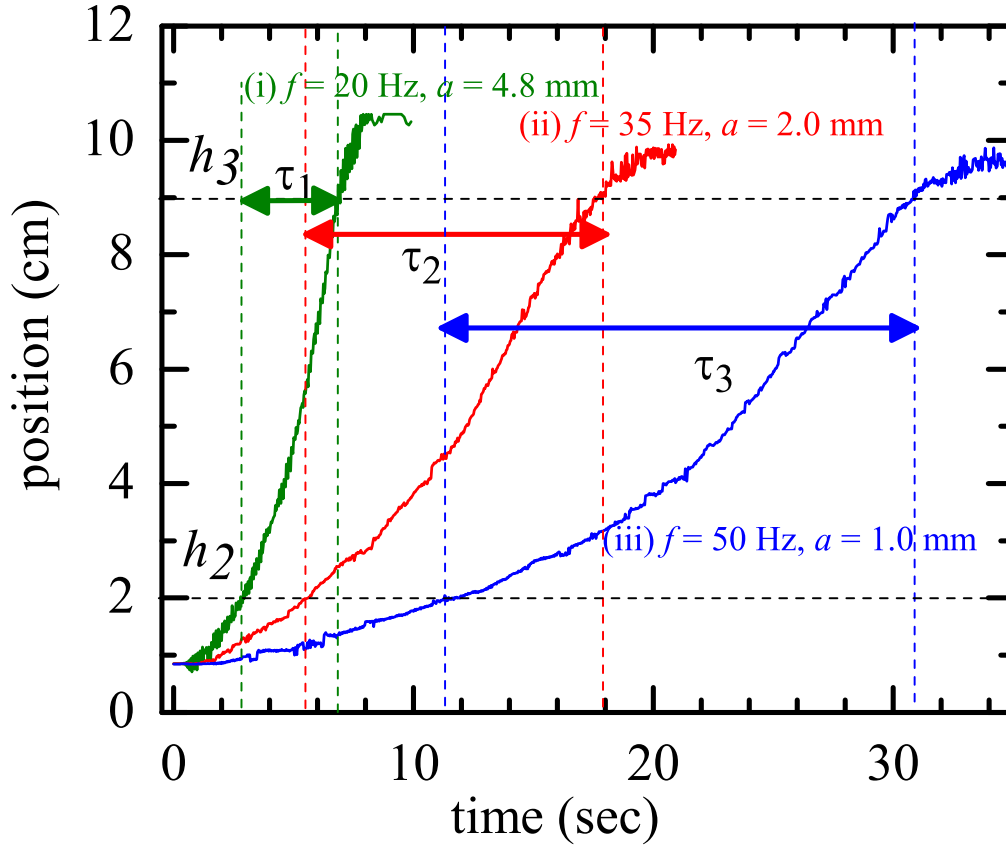


FIG. 6: **Intruder position vs. time plot.** Position vs. time plots for an intruder of $\rho_r = 1.07$, for i) $f = 20$ Hz, $a = 4.8$ mm (green), ii) $f = 35$ Hz, $a = 2.0$ mm (red) and $f = 50$ Hz, $a = 1.2$ mm (blue). The bed-height was 10 cm and width was 13 cm and the sidewall roughness was $P - 100$ sandpaper. The dashed horizontal lines (black) represent h_2 and h_3 (see Fig. 1a of main paper). The rise-time of the particle is computed by estimating the time it takes for the intruder to rise from the position h_2 to h_3 . The vertical dashed lines in green, red and blue enclose the time windows required by the intruder to rise between h_2 and h_3 for the three shaking experiments (i), (ii) and (iii) respectively.

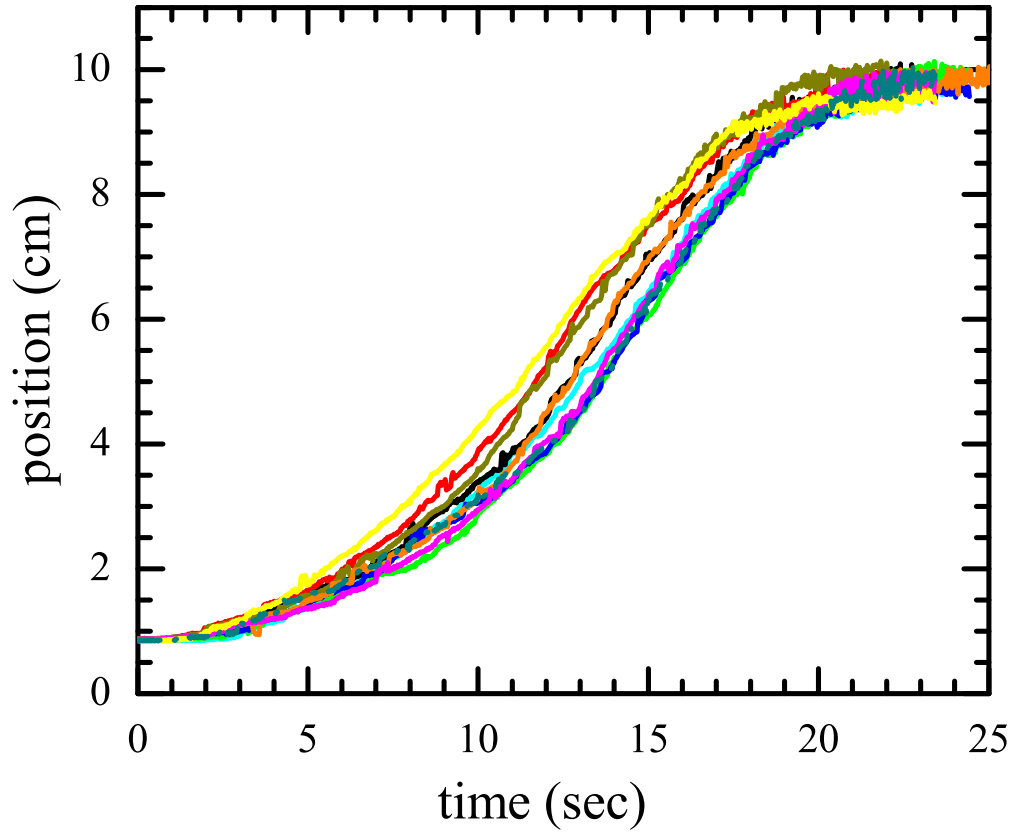


FIG. 7: **Different realizations of intruder trajectories.** Position vs. time plots for 10 different trials of the rise of a $\rho_r = 1.07$ intruder for $f = 50$ Hz and $a = 1.4$ mm. The bed-height was 10 cm and width was 13 cm and the sidewall was roughened with P-100 sandpaper. The trajectories show roughly quadratic dependence on time. The different repeats of the experiment for fixed control parameters lead to slightly different trajectories and hence small fluctuations of rise-times over different realizations.

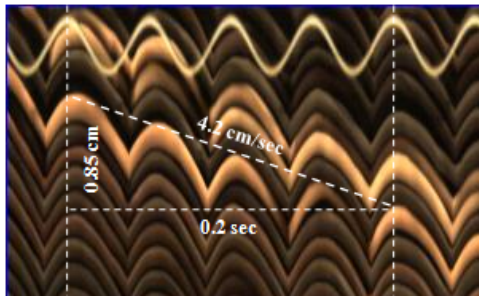
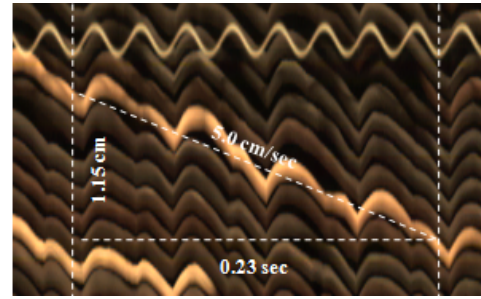
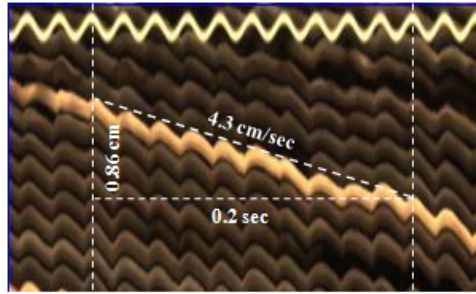
(a) $f = 20$ Hz, $a = 3.7$ mm, $a\omega = 46.5$ cm/sec(b) $f = 35$ Hz, $a = 2.1$ mm, $a\omega = 46.2$ cm/sec(c) $f = 50$ Hz, $a = 1.5$ mm, $a\omega = 47.1$ cm/sec

FIG. 8: (Color online) Tagged particle trajectories (y -vs- t) near wall. Each bright, slanted yellow trajectory represents the time-evolution of the y (vertical)-coordinate of a tagged particle (yellow mustard seed) adjacent to the side wall, for three different parameter sets. The slope of the yellow trajectory gives the velocity of the tagged particles as (a) 4.2 cm/sec, (b) 5.0 cm/sec and (c) 4.3 cm/sec respectively. The white sinusoidal trace (horizontal) represents the time-evolution of a reference white mark on the acrylic cell.

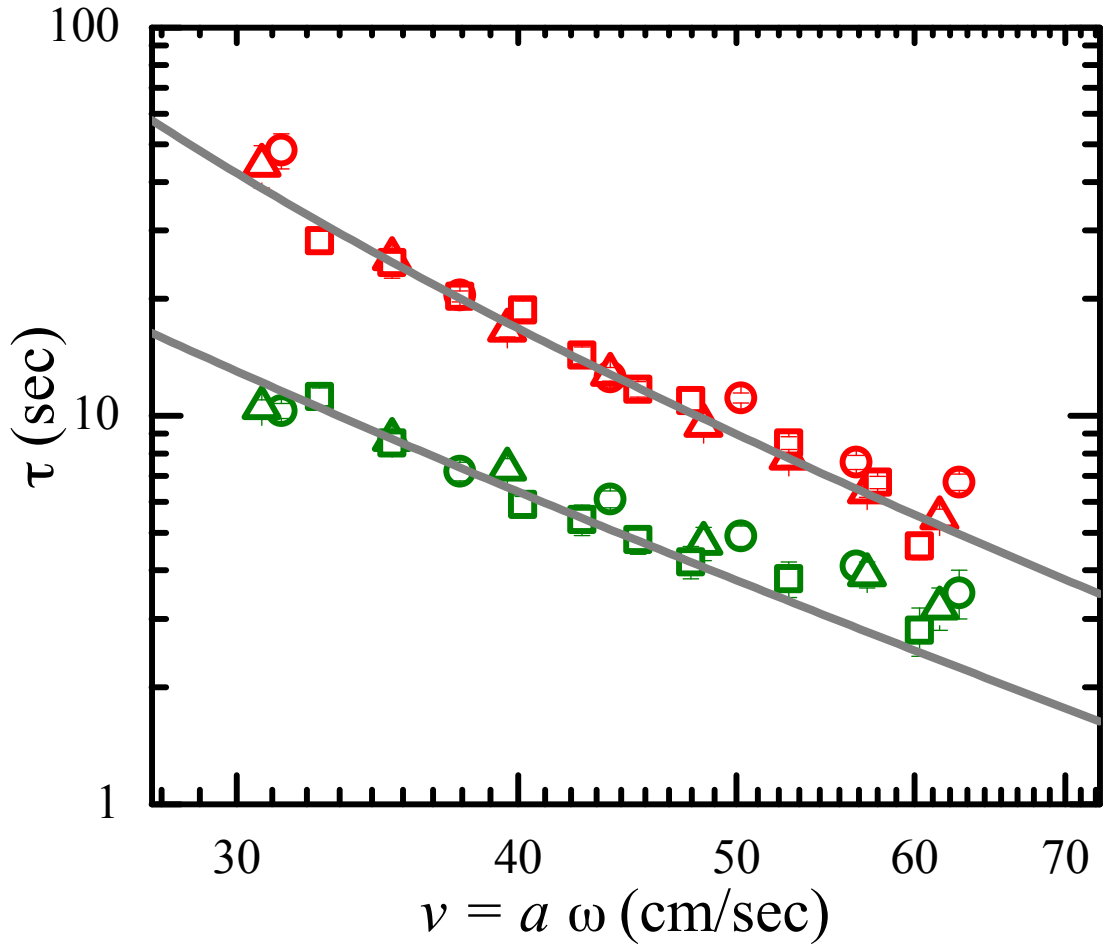


FIG. 9: **Plots of the rise-time for different bed-heights.** Plot of τ versus $v = a\omega$ for two different bed heights $h = 8$ cm (green) and $h = 10$ cm (red), for three different frequencies 20 Hz (\square), 35 Hz (\triangle) and 50 Hz (\circ). The bed-width was 13 cm and the sidewall roughness was achieved with P-100 sandpaper. In all experiments, the relative density was $\rho_r = 1.07$ and the intruder size was 1.7 cm. We see good collapse of data for both heights. The fits are to the scaling form $A(v - v_c)^{-2}$ with $A \approx 13000$ cm²/sec, $v_c \approx 15$ cm/sec for the 10 cm bed and $A \approx 7000$ cm²/sec, $v_c \approx 7$ cm/sec for the 8 cm bed.

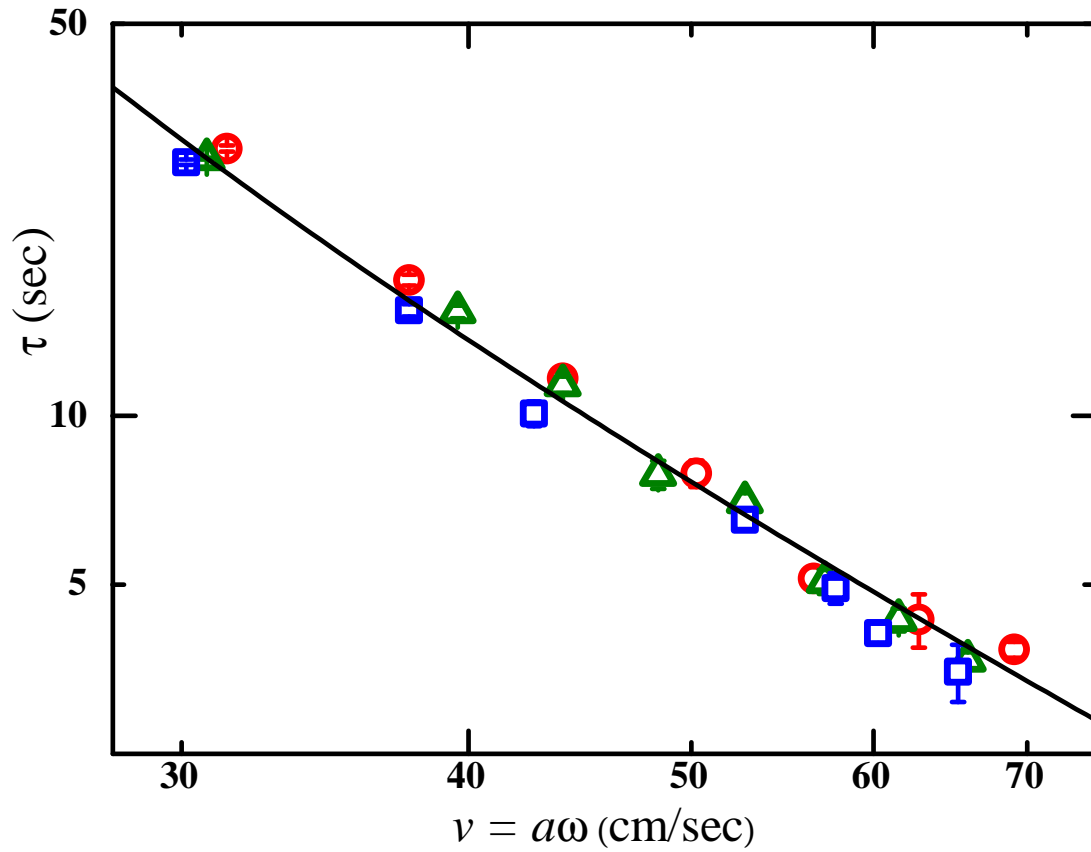


FIG. 10: **Plots of the rise-time for a different choice of bed-particles.** Here the bed particles were fenugreek seeds that are larger, have different shapes and are characterized by higher size polydispersity than the mustard seeds. The bed-height was $h = 10$ cm, bed-width 13 cm, sandpaper roughness $P = 100$ and the data is for three different frequencies 20 Hz (\square), 35 Hz (\triangle) and 50 Hz (\circ). The intruder had a diameter 1.7 cm, thickness 5 mm and density 1.07 g/cc.

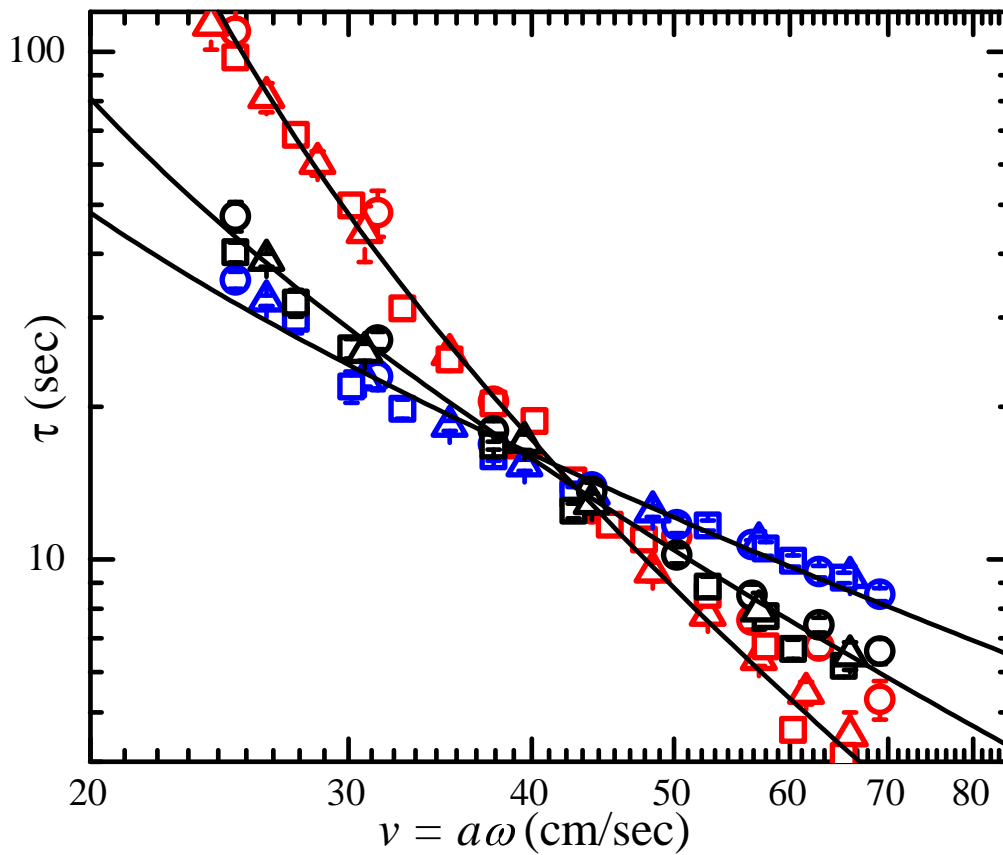


FIG. 11: **Plots of the rise-times for three different bed-widths.** The data sets correspond to the cell widths 13 cm (red), 15.5 cm (black) and 18 cm (blue), for three different frequencies 20 Hz (\square), 35 Hz (\triangle) and 50 Hz (\circ). The bed-particles were mustard seeds, cell-height was 10 cm and sidewall sandpaper roughness $P = 100$. The intruder had a diameter 1.7 cm, thickness 5 mm and density 1.07 g/cc. The solid lines correspond to the scaling form $(v - v_c)^{-\alpha}$ with $\alpha = 2.0, 1.4$ and 1.0 respectively.

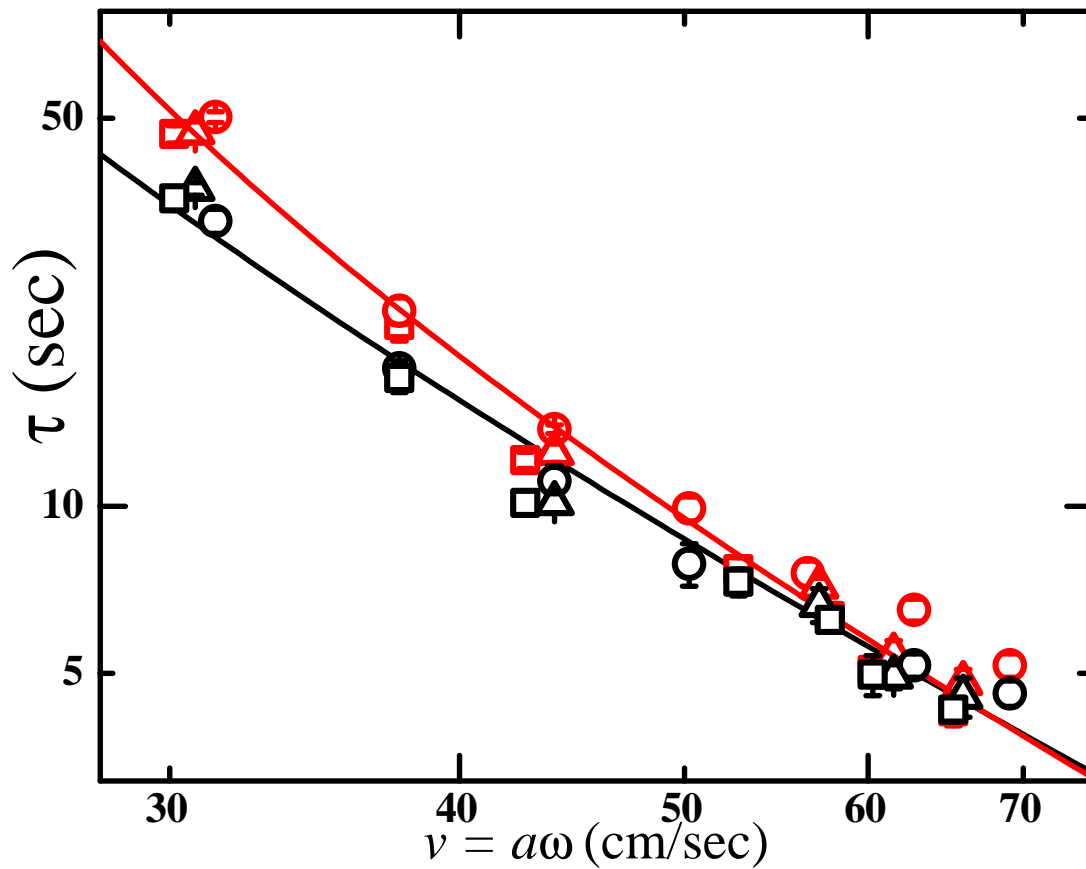


FIG. 12: **Plots of the rise-times for two different side-wall roughnesses.** Here we show the rise-time data for two different wall roughness using sandpaper with ISO grit designations $P - 100$ (red) and $P - 60$ (black). The bed-particles were mustard seeds, cell-height was 10 cm and bed-width was 13 cm. The intruder had a diameter 1.7 cm, thickness 5 mm and density 1.07 g/cc. The solid lines correspond to the scaling form $(v - v_c)^{-2}$ with $v_c = 15$ cm/sec and 10 cm/sec respectively.